ROYAL SOCIETY OF CHEMISTRY

Check for updates

A smart diagnostic tool based on deep kernel learning for on-site determination of phosphate, calcium, and magnesium concentration in a hydroponic system

Vu Ngoc Tuan, [ID] [abc] Trinh Dinh Dinh, [ID] [de] Wenxin Zhang, [ab] Abdul Mateen Khattak, [bf] Anh Tuan Le, [bc] Iftikhar Ahmed Saeed, [ag] Wanlin Gao*[ab] and Minjuan Wang*[ab]

Calcium, phosphate, and magnesium are essential nutrients for plant growth. The *in situ* determination of these nutrients is an important task for monitoring them in a closed hydroponic system where the nutrient elements need to be individually quantified based on ion-selective electrode (ISE) sensing. The accuracy issue of calcium ISEs due to interference, drift, and ionic strength, and the unavailability of phosphate and magnesium ISEs makes the development of these ion detecting tools hard to set up in a hydroponic system. This study modeled and evaluated a smart tool for recognising three ions (calcium, phosphate, and magnesium) based on the automatic multivariate standard addition method (AMSAM) and deep kernel learning (DKL) model. The purpose was to improve the accuracy of calcium ISEs, determining phosphate through cobalt electrochemistry, and soft sensing of magnesium ions. The model provided better performance in on-site detecting and measuring those ions in a lettuce hydroponic system achieving root mean square errors (RMSEs) of 12.5, 12.1, and 7.5 mg L^{-1} with coefficients of variation (CVs) below 5.0%, 7.0%, and 10% for determining Ca^{2+}, $H_2PO_4^-$, and Mg^{2+} in the range of 150–250, 100–200, and 20–70 mg L^{-1} respectively. Furthermore, the DKL was implemented for the first time in the third platform (LabVIEW) and deployed to determine three ions in a real on-site hydroponic system. The open architecture of the SDT allowed posting the measured results on a cloud computer. This would help growers monitor their plants' nutrients conveniently. The informative data about the three mentioned ions that have no commercial sensors so far, could be adapted to the other components to develop a fully automated fertigation system for hydroponic production.

1. Introduction

Managing nutrients and monitoring plant growth in a hydroponic system are essential tasks in the modern farming industries. In a soilless cultivation, the total nutrient can be easily manipulated by regularizing electrical conductivity (EC) and pH values. However, the EC, pH based hydroponic systems have issues of imbalanced nutrients caused by the unequal uptake of nutrient ions from a hydroponic solution by different plants species. This is one of the major reasons for reduction in crop productivity and quality in the closed-loop hydroponic systems.[1] Therefore, the nutrient management systems need to be equipped with real-time diagnostics, controlling essential nutrient elements individually. Thus far, such a system is not available commercially because of the lack of feasible ISEs, and the complexity of the on-site measurement of individual ions.

A periodical analysis was used as a temporary solution to minimize imbalance in nutrients by adjusting nutrient ratios in the solutions.[2] However, this method was inefficient to induce extra water and loss of nutrient control because of no real-time feedback. The ISEs were used as an efficient method to overcome this problem. They supply timely feedback to the system on individual ions for on-line regularization of ion ratio in the nutrient solution. Nevertheless, the ISEs based hydroponic systems face other problems, such as interferences (other ions, temperature), changing ionic strength, potential drifts, *etc.* These negative impacts reduce the accuracy of ISEs measurements and the efficiency of ISEs-based closed-loop hydroponic

[a] Key Laboratory of Agricultural Informatization Standardization, Ministry of Agriculture and Rural Affairs, Beijing 100083, China

[b] College of Information and Electrical Engineering, China Agricultural University, Beijing 100083, China. E-mail: minjuan@cau.edu.cn; gaowlin@cau.edu.cn

[c] Faculty of Electrical and Electronic Engineering, Nam Dinh University of Technology Education, Nam Dinh 420000, Vietnam

[d] Quality Testing Lab, Center for Research and Development Science Technology Tien Nong, Thanh Hoa, 442410, Vietnam

[e] College of Chemistry and Chemical Engineering, Beijing Institute of Technology, Beijing, 102488, China

[f] Department of Horticulture, The University of Agriculture, Peshawar 25120, Pakistan

[g] Department of Computer Science, The University of Lahore, Pakistan

systems. Especially, a substantial impact is observed on bivalent ions, such as, calcium and magnesium. In this regard, several solutions for improving the accuracy of calcium ISE were proposed. These include, using calibration techniques to reduce drift,[3–5] using machine learning techniques (PLS, PCR) to resolve interferences,[6] deploying neural network,[7] applying the sampling technique and the processing model.[4,8] A combination of the sampling technique and advanced model was recently proposed to overcome interferences, drift, and ionic strength.[4] However, calcium is a major element that plants require and is difficult to measure with high accuracy in a hydroponic solution, especially in the on-site scenario. Therefore, further validation needs to be done to measure calcium ion with high precision in a hydroponic solution.

Phosphate is one of the essential plants nutrients that needs to be diagnosed in the hydroponic solution for precision cultivation. Although various studies have focused on developing phosphate sensing, only a few have been able to directly measure phosphate because of its short lifetime, drastically losing sensitivity,[9] and crucial interference of other ions.[10] Cobalt-wire (Co) was a significant milestone for developing a phosphate selective electrode. It was quite useful in field analyses[11] and was cheap, simple, and robust. However, in the wide range of pH states, phosphate anion species (PO_4^{3-}, HPO_4^{2-}, $H_2PO_4^-$) changed, which affected the accuracy phosphate detection. Therefore, quantifying phosphate ion concentration in a hydroponics solution is complicated and less accurate, even with a Co-based electrode[10] due to the unstable electrode signal band. Several approaches have been devised to resolve this issue, such as sensing data fusion for detecting $H_2PO_4^-$ concentration in a paprika nutrient solution based on the near-infrared (NIR) spectroscopy technique, cobalt electrochemistry, and artificial neural network (ANN) model.[12] Spectroscopy sensing technique aided with the machine learning models is a relatively satisfactory method to detect phosphate ion. However, it is expensive and infeasible for the on-line measurement system.[13] Recently Tuan *et al.*[14] proposed an approach combining the multivariate standard addition sampling method and the ANN model for data fusion of four cobalt electrodes. They achieved satisfactory results in determining phosphate ion in eggplant hydroponic solution. Nonetheless, an on-line and feasible phosphate measurement system has not been proposed yet.

Like phosphate, there were many obstacles in developing magnesium ion sensing mechanisms. Several studies devised ionophores for detecting magnesium.[15–17] However, due to drift and interference of other ions such as calcium, sulphate, *etc.*, no commercial magnesium ISE was introduced for determining Mg^{2+} efficiently. This inspired researchers to develop magnesium sensing more efficiently by applying the ISEs with advanced processing techniques. For example, using a solid contact ISE array supported by independent component analysis (ICA) with the genetic algorithm and back-propagation neural network (BPNN).[18] This study achieved comparable results. However, it also used complicated processing methods and only worked well in an ideal environmental scenario, where pH, ion strength, temperature, and other forms of interference

(from unknown ions) were relatively constant. Atas *et al.*[19] proposed an ISE array electronic tongue that supported the partial least squares (PLS) model for determining magnesium and other elements in solution samples. This provided satisfactory results in determining magnesium, as well as, calcium. However, this approach is still challenging as the lifetime of the electrode is very limited (to almost a single analysis). The analysis time is extended using of a number of solutions. Some studies were recently proposed that combined special sampling techniques and advanced processing models to predict magnesium and phosphate from the raw data of an array of ISEs of other ions. For example, Cho *et al.*[8] used the two-point sampling procedure and ANN to predict the concerned ions from a three ISEs array. However, the prediction magnesium and phosphate detection of the study did not meet the requirements of the actual hydroponic system. Tuan *et al.*[4] combined the multivariate variate standard addition method (MSAM) and the deep kernel learning (DKL) model to improve the prediction results of two unavailable ions (magnesium and phosphate) and six other available ISEs ions. This approach provided a relatively comprehensive solution to resolve the problems of ISEs. With the model, although the prediction of phosphate and magnesium improved considerably, the results are still incomparable with those achieved through actual ISEs. Moreover, the DKL based model of that study was slightly complicated (especially in the case of big data). Implementing DKL in the on-site measurement system has been a challenge because of the computational cost of DKL core. No DKL model has been introduced in the actual system, *i.e.* the real hydroponic system. Therefore, deploying ISEs and DKL in hydroponics need further studies on evaluating their feasibility in real-time and on-site nutrients monitoring in hydroponic systems.

This study proposes a smart diagnostic tool (SDT) for on-site determination of three essential ions in a lettuce hydroponic solution. The multivariate standard addition sampling technique[14] was applied to acquire data from one calcium ISE, four cobalt-based phosphate ISEs, and one temperature probe. The DKL, novel processing model,[4] was used to improve the accuracies of Ca^{2+}, $H_2PO_4^-$ ISEs and enhance performance of Mg^{2+} ion prediction. The proposed model was trained and validated with 100 imitated real hydroponic solution samples in a Python environment. The sampling procedure based on the automated multivariate standard addition method (AMSAM) and trained DKL model were implemented in LabVIEW program for real-time monitoring concentrations of three ions in the hydroponic solution. Implementing a smart diagnostic tool based on the automated multivariate standard addition method (AMSAM) and DKL in LabVIEW is a novel approach for on-site monitoring of ions concentration in a hydroponic system. The computational challenge of applying the DKL model in the on-site monitoring system was alleviated by optimizing and implementing the fitted architecture in LabVIEW. Moreover, the predicted concentration values are also posted to the cloud computing as an online database. This cloud database was developed to validate the feasibility of this study in the real hydroponic system, where several modules continuously exchange data and supply information to manage the entire system (Fig. 1).
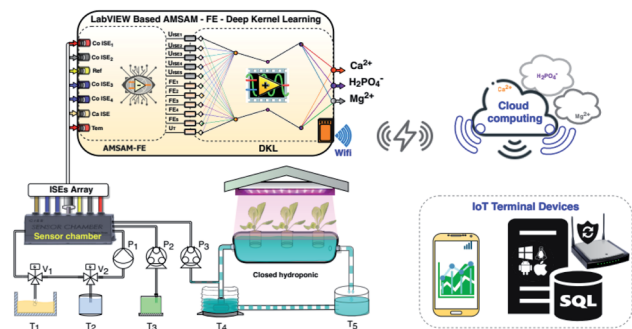
Fig. 1 The novel smart diagnostic tool (SDT) based on AMSAM-FE-deep kernel learning for determining calcium, phosphate, and magnesium concentration in a hydroponic system.

2. Materials and methods

2.1. Experiment preparation

2.1.1. Sensor array and apparatus. A sensor array was set up with 5 sensors, including a commercial ISE Orion 9320BNWP (Thermo Fisher Scientific, USA), which was used for determining calcium ion. Four ISEs were fabricated from a cobalt rod (99.99% pure, 5 mm diameter, Sigma-Aldrich, USA) for sensing phosphate. For the phosphate electrodes fabrication, a 5 mm long cobalt rod was soldered to a copper wire ($\varnothing = 1$ mm). The bimetal structure (cobalt–copper) was covered by an acrylonitrile butadiene styrene (ABS) plastic stem (a 3D printed pipe with 100 mm length, 12 mm external diameter, and 6 mm internal diameter). The Bayonet Neill–Concelman (BNC) cable was jointed with metallic ISEs for convenience in connection.[14] The 400 and 1200 grit emery papers were utilized to polish the electrodes. Further, the electrodes were pre-treated with distilled water for 30 minutes and then conditioned in potassium hydrogen phthalate buffer (KHP) 0.04 mol L^{-1} for 20 minutes.[20] The formed electromotive forces (EMF) between a reference electrode (Orion 900200, Thermo Fisher, MA, USA) and the activated cobalt electrodes were collected for determining phosphate concentration. The temperature of samples was detected by a temperature probe (Pt100; Yuace, China). All of the sensors were plugged into an ABS-sensor chamber (a 3D-

printer lab product). The sensor chamber was adapted with other components, such as electromagnetic valves (V_1, V_2), electric pump (P_1), and peristaltic pumps (P_2, P_3) to form an automated sampling system based on the MSAM technique.[14] The solutions, including waste, deionized water, KHP, real hydroponic nutrient solution, cycled hydroponic nutrient solution, were kept in tanks T_1, T_2, T_3, T_4, and T_5, respectively. The base characteristics of sensors and apparatus are summarized in Table 1. The array sensors were connected to an INA 116 (Texas Instruments, USA) based conditioning amplifier. A data acquisition device (NI USB DAQ 6218 National Instrument Corporation, USA) was used to acquire and transfer data to a computer. A smart diagnostic program based on DKL implemented in LabVIEW (LabVIEW 2017, National Instrument Corporation, USA) was utilized to process data and quantify the concentration of the three considered ions (Fig. 1).

Fig. 2 depicts the progress to develop a smart diagnostic tool to determine three ions in a hydroponic system. The process of developing SDT was divided into two parts, (i) modeling the DKL core model of SDT in Python environment and (ii) implementing the automated multivariate standard addition sampling module and DKL in LabVIEW platform. In the Python environment, the training samples were prepared manually, acquired by a task in the LabVIEW program first, and the data were exported to a comma-separated-values (CSV) file for the DKL model training. To improve the model performance, the raw data features were enriched deploying the feature enrichment technique,[14] explained in Section 2.2.2. The dataset was then normalized into a range of [−1, 1] to increase training speed. The normalized dataset was introduced to develop the DKL model. The DKL model was trained, tested, and evaluated by a modeling program based on Python and several Libraries. The trained parameters (including weights, biases, and kernel matrices) were exported to .txt files for implementing the DKL in LabVIEW. In the LabVIEW platform, an automated sampling module based on multivariate standard addition method-MSAM[4,14] was developed for an on-site measurement in the actual hydroponic system (see the detail of this module in Section 2.2.1). The samples were enriched with features, normalized, and introduced into the DKL implemented in

Table 1 Characteristics of the ISEs, sensors, and other components used in the study

Components	Specification	Manufacturer
Calcium ISE: Orion 9720BNWP	0.02–40 000 mg L^{-1}; PVC membrane	Thermo Fisher, USA
Phosphate ISE$_1$	Co-metal membrane	Lab design
Phosphate ISE$_2$	Co-metal membrane	Lab design
Phosphate ISE$_3$	Co-metal membrane	Lab design
Phosphate ISE$_4$	Co-metal membrane	Lab design
Reference electrode: Orion 900200	Double conjunction electrode	Thermo Fisher, USA
Temperature probe: Pt100	0–100 °C; power 24VDC	Yuace, China
Electromagnetic valve (V_1, V_2)	FFY23 series TR-6; 24VDC	Wuxi Teradyne, China
Electric pump (P_1)	KLP05-6; power 6VDC; flow rate 450 mL min^{-1}	Kamoer, China
Peristaltic pump A (P_2)	NKP-DA-S10B; power 24VDC; flow rate 80 mL min^{-1}	Kamoer, China
Peristaltic pump B (P_3)	S300-2B-JZ15B; power 24VDC; flow rate 192.39 mL min^{-1}	Di Chuang, China
Acquisition device	NI USB 6218	National Instrument Corporation, USA
Buffer ISEs' signals	INA116	Texas Instrument, USA

LabVIEW. The DKL predicts and transfers the outcome of the considered ions concentration *via* the un-normalized processing. The concentrations of three ions are displayed and also posted to the cloud computing database of ThingSpeak[21] open service (Matwork, Natick, MA, USA) for distributed monitoring and manipulating purposes. The real concentration values of the actual samples were analyzed at the Laboratory of Agricultural Informatization Standardization, Ministry of Agriculture and Rural Affairs, CAU, Beijing, China, at the International Joint Research Center of Aerospace Biotechnology and Medical Engineering, Beihang University, Beijing, China, and at Quality Testing Lab, Center for Research and Development Science Technology Tien Nong, Thanh Hoa, Vietnam.

2.1.2. Sample preparation. Training samples for developing the DKL-core of the smart diagnostic tool was prepared from standard solutions in the laboratory. Then SDT was validated by on-site monitoring of three target ions to verify the feasibility of the SDT structure in the real hydroponic systems (Fig. 3). To imitate the interaction of matrix ions of the hydroponic solution, a basic solution (BS) mixed as per the Hoagland standard solution[22] and tap water (1/1 v/v), was used to prepare the training samples. The fractional factorial design (FFD)

method[23,24] was deployed to prepare 100 training samples (100 = 10^2, for 10 levels of three factors-3 ions, as shown in Table 2). The temperature of samples was randomly adjusted from 15 °C to 33 °C (corresponding to the temperature of real hydroponic systems) using a water bath HH.S21-4 (Boxun, Shanghai, China) for eliminating temperature interference.

To mimic the matrix background of real hydroponic samples, a basic solution (BS), mixing Hoagland standard solution[22] and tap water (1/1 v/v), was used to prepare the training samples. Standard solutions (SS) of 10 mL were prepared by mixing BS solution with appropriate amounts of stock solutions of potassium dihydrogen phosphate, magnesium sulfate, calcium nitrate to range the concentration of concerned ions from the first to the tenth level of 10–350, 10–668 mg L^{-1}, and 5–125 mg L^{-1} for Ca^{2+}, $H_2PO_4^-$, and Mg^{2+}, respectively (Table 2). A training sample set for developing the proposed model, having 100 samples, was prepared by using the MSAM technique. KHP buffer solution (25 mL, 0.035 M) was first injected into the sensor chamber. The solution inside the sensor chamber was then cycled by an electric pump (KLP05-6, Kamoer Company, China) until the ISEs' EMFs (U_0) were
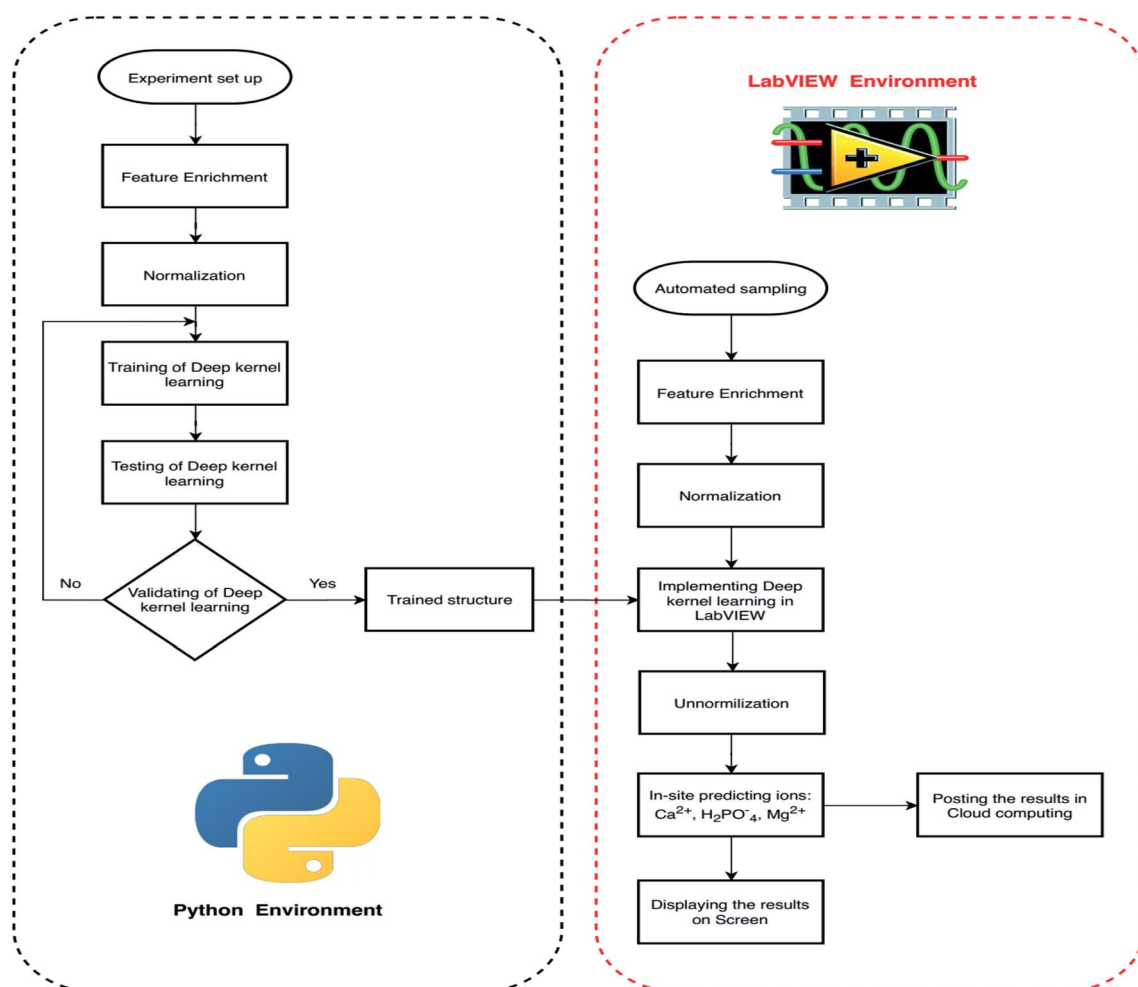

Fig. 2 Flow chart of progress in Python and LabVIEW environments to develop a smart diagnostic tool for determining three ions (calcium, phosphate, and magnesium) in a hydroponic system.
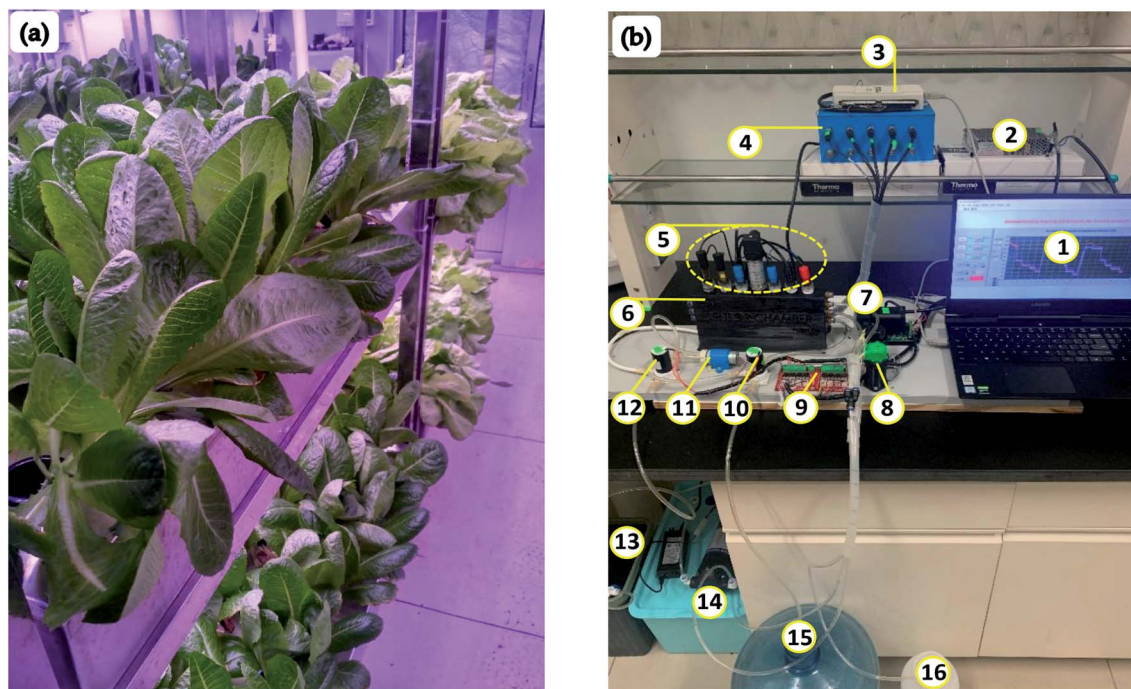
Fig. 3 Lettuce plants growing in a plant factory (a) and the on-site measurement system used in the study (b). (1) Computer with DKL based SDT model; (2) power supply; (3) NI 6218 DAQ device; (4) ISEs interfacing module; (5) sensors array; (6) sensor chamber; (7) peristaltic pump B; (8) peristaltic pump A; (9) driver board of pumps and valves; (10) magnetic valve 1; (11) electric pump; (12) magnetic valve 2; (13) waste tank; (14) sample tank; (15) distilled water tank; (16) KHP tank.

stabilized (about 60 seconds). The standard solution was injected into the chamber. For 3 minutes of cycling, the potentials of the electrodes (U_x) were stabilized. The data acquisition program based on LabVIEW (LabVIEW 2017, National Instrument Corporation, USA) collected the stabilized EMF values and exported them to the CSV file for developing the model. The DKL model was developed by Python 3.6.2, Scikit-Learn library, SciPy, and several third-party libraries, and then implemented by using LabVIEW for the on-site monitoring stage (Fig. 3).

2.2. Development of the smart diagnostic tool

2.2.1. Developing automated multivariate standard addition sampling module. The timing diagram of an automated multivariate standard addition method (AMSAM) is illustrated in Fig. 4 (for 1 cycle). One sample was acquired in 1 cycle. At t_1 a starting pulse from the main program activated the AMSAM to sample. P_1 and P_2 were turned on, for Δt_1 (30 seconds) to pump the buffer solution from the KHP tank (T_3), P_2 was turned off (to get 25 mL volume of the KHP). After 60 seconds (Δt_2) from starting pulse, the KHP was cycled by P_1, during which the DAQ

device acquired stable potentials from the electrodes (U_0). The pump P_3 was then activated (at t_3) and maintained for 30 seconds (Δt_3) for pumping the real hydroponic sample solution (10 mL) from the real hydroponic solution tank (T_4) to the sensor chamber. The combined solution in the sensor chamber was mixed and cycled for 180 seconds (Δt_4) till the electrodes' signals were stable. The EMFs of electrodes (U_x) were collected. The potentials (U_0) and (U_x) were then introduced to the next step for feature enrichment, normalization, and prediction, *etc.*, (Fig. 2). At t_5 electromagnetic valve V_1 was activated for 30 seconds (Δt_5), the measured sample was drained out of the sensor chamber to the waste tank (T_1). At t_5 switching off V_1 and on V_2 stopped draining and started rinsing solution from the water tank (T_3) to the sensor chamber for 30 seconds (Δt_6), then the sensor array rinsed for 30 seconds (Δt_7). At t_7 when the rinsing completed, the draining V_1 was turned on again to drain the wastewater out of the sensor array for 30 seconds (Δt_8). At t_9 both pump P_1 and electromagnetic valve V_1 were stopped to finish one automated sampling cycle. The main program can call the automated sampling cycle to acquire the signals of the real sample.

Table 2 The ranges concentration of three considered ions prepared training samples

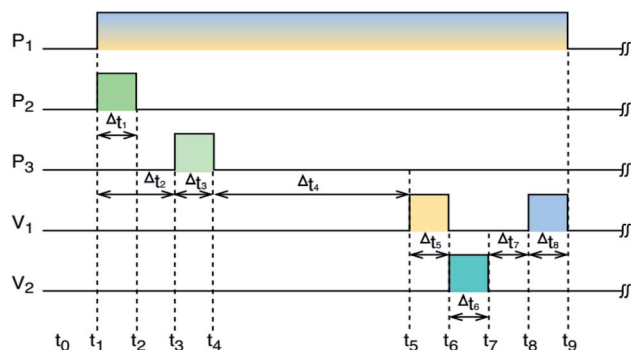| Ions	Level 1	Level 2	Level 3	Level 4	Level 5	Level 6	Level 7	Level 8	Level 9	Level 10
Calcium (mg L^{-1})	10	25	50	75	100	125	175	225	275	350
Phosphate (mg L^{-1})	10	20	45	70	100	150	225	350	500	668
Magnesium (mg L^{-1})	5	15	25	35	45	55	70	85	105	125

Fig. 4 The timing diagram of the automated multivariate standard addition method (AMSAM) processing.

2.2.2. The signal processing model of the smart diagnostic tool.

The SDT was developed based on an automated novel sampling technique-AMSAM and an advanced signal processing model-DKL. This way, the DKL model was used to resolve the problems of ISEs (interferences, drift, *etc.*). Moreover, the data provided by the automated multivariate standard addition method (AMSAM) based on MSAM[4,14] was the foundation for reducing ionic strength and drift effects. The raw dataset was acquired from the sensor array. DKL model was an elegant and flexible algorithm,[25] a combined structure of deep neural network and kernel methods. The DKL and AMSAM were applied to develop a smart diagnostic tool for determining on-site concentrations of the three ions in a hydroponic nutrient solution. The 11 feature (including 5 raw ISEs' signals, 5 enriched ISEs' signals, and one temperature signal) dataset was introduced to the DKL, which was improved to supply useful information using the feature enrichment technique.[14] The enriched principle is performed as in eqn (1) and depicted in Fig. 1. Ten data features were formed from five original features (5 ISEs' EMFs) and five feature enrichment (FE) data.

$$U_{\mathrm{FE}ij} = U_{xij} - U_{0ij} \tag{1}$$

where i, j – the index of samples (1 to 100), and the ion-selective electrodes (1 to 5), respectively. U_{0ij}, U_{xij} – the ISEs' potentials corresponding to the concentration C_0 and C_x respectively. $U_{\mathrm{FE}ij}$ - the values of the difference between U_{0ij} and U_{xij} (enriched data values) were used to improve the performance of the model. See ref. 14 for more information on this technique.

The DKL was modeled by the cross-validation technique with k-fold ($k = 10$). The dataset was divided into a training set $D = \{X^i, y^i\}$, $i = 1, 2, \ldots, n$ and a testing set $D_* = \{X_*^k, y_*^k\}$, $k = 1, 2, \ldots, n_*$. The Gaussian process was defined by three covariance matrices

$K(X,X)$ at training locations X, $K(X_*,X_*)$ at testing locations, and $K(X_*,X)$ at training locations and testing locations.[26]

$$\begin{bmatrix} f(X) \\ f(X_*) \end{bmatrix} \sim N\left(0, \begin{bmatrix} K(X, X) & K(X, X_*) \\ K(X_*, X) & K(X_*, X_*) \end{bmatrix}\right) \tag{2}$$

The GP stage in DKL has a functional equivalent as an infinite number of nodes Bayesian neural network.[27] Therefore, the posterior distribution of the input data was used to predict the expected target ions.

$$f(X_*)|y(X) \sim N(\mu_*, \Sigma_*) \tag{3}$$

where μ_* was the predictive mean and calculated as follows[26]

$$\mu_* = m(X_*) + K(X_*,X)[K(X,X) + \sigma^2 I]^{-1}(y(X) - m(X)) \tag{4}$$

$$\mu_* = f(X_*) = K(X_*,X)[K(X,X) + \sigma^2 I]^{-1} y(X) \tag{5}$$

Eqn (5) was used to compute the prediction of the outputs of DKL. To conveniently implement the DKL and calculate the predictions in a different environment (for example, LabVIEW), we can compute the predictions as follows[26]

$$\mu_* = f(X_*) = K(X_*,X)\alpha \tag{6}$$

where $\alpha = [K(X,X) + \sigma^2 I]^{-1} y(X)$, the trained parameters from the program in the training environment (Python).

The given data were processed in two stages. First, in the forward stage of the neural network, the high-dimensional input vector was propagated to the lower-dimensional vector. The low-dimensional data were then processed by the GP stage. The DKL architecture is also considered as a stand-alone deep kernel-based GP.[25] Thus we can use expression (7) to describe the structure of DKL with a base kernel $k(x^{[i]}, x^{[j]}|\theta)$ and kernel parameters θ.

$$k(x^{[i]}, x^{[j]}|\theta) \rightarrow k(g(x^{[i]}, w), g(x^{[j]}, w)|\theta, w) \tag{7}$$

The neural network performs a non-linear mapping by $g(x,w)$, and the weight parameter (w). Kernel RBF, dot-product, and Matérn kernel (Table 3) were used to estimate the fitted architecture of the DKL model. The maximizing log marginal likelihood of the targets y was used to perform kernel learning algorism for DKL. The probability of the data conditioned only on kernel parameters θ is given as;

$$\log p(Y|\theta,X) \propto -Y^{\mathrm{T}}(K_\theta(X,X) + \sigma^2 I)^{-1} Y - \log|K_\theta(X,X) + \sigma^2 I| \tag{8}$$

Table 3 The kernels used to develop the DKL core of the SDT in this study

Kernels	Radial basic function (RBF)	Dot-Product	Matérn kernel
Function	$k(x, x') = \exp\left[\dfrac{-(x - x')^2}{2l^2}\right]$ l is length-scale	$k(x,x') = x.x'$	$k(x, x') = \dfrac{1}{\Gamma(v)2^{v-1}}\left(\dfrac{\sqrt{2v}}{l}\mathrm{d}(x, x')\right)^v K_v\left(\dfrac{\sqrt{2v}}{l}\mathrm{d}(x, x')\right)$ l – length-scale; v – const; $\mathrm{d}(x,x')$ – Euclidean distance; K_v – modified Bessel function; Γ – gamma function

Table 4 The considered parameters for developing the DKL core of the smart diagnostic tool

Parameters	Values
Number of layers	1, 2, 3, 4, 5, 6
Size of hidden layer	1 to 1000
Transfer function $f(x)$ of hidden layers	Tansig, logsig, linear, ReLU
Transfer function of the output layer	ReLU
Optimization algorithm	Stochastic gradient descent (SGD), Broyden–Fletcher–Goldfarb–Shanno (BFGS), Adam
Dropout rate	0.5 to 0.99
Learning rate	0.001 to 0.1
Max number of epochs	2000
Prior white noise level	0.001 to 1
Kernel	Radial basic function (RBF), dot-product, Matérn kernel
Training goal	10^{-6}

Modelling DKL concerns optimizing learnable parameters, such as network weights and kernel parameters, and tweaking the hyper-parameters, *i.e.*, the learning rate, number of iterations, and number of neurons (nodes) in each layer of the neural network. First, the hyper-parameters were chosen with appropriate values. Cross-validation over a small hyper-parameter search-space and

a systematic optimization-based procedure was then applied to train the model. The main hyper-parameters were tuned, including the number of neurons of each hidden layer, the number of epochs, training iterations, the learning rate, and the prior white-noise level of the Gaussian process (Table 4).

The parameters of the neural stage (w) and kernel parameters of GP (θ) were jointed to all parameters of the DKL, $\gamma = \{w, \theta\}$, and eqn (8) was deployed to maximize the log posterior marginal likelihood. The standard back-propagation technique was employed to compute the derivatives concerning the weight variables $\frac{\partial g(x, w)}{\partial w}$. The dropout algorithm was used to resolve the overfitting and local minima problems. The dropout rate ranged from 0.5 to 0.99.[28]

3. Results

3.1. Determining the core structure of the smart diagnostic tool

DKL model is the core of the smart diagnostic tool. Numerous trials were conducted to determine the major parameters and the hyper-parameters network (Table 4) for the best-fit DKL architecture. Five DKL core structures were considered (Table 5). The DKL model structure was tuned within five layers of the neural network and an RBF kernel-based Gaussian process. The

Table 5 The structures of the DKL models for coring the smart diagnostic tool (SDT)[a]

Models	Layer 1 N.o.N	AF	DR	Layer 2 N.o.N	AF	DR	Layer 3 N.o.N	AF	DR	Layer 4 N.o.N	AF	DR	Layer 5 N.o.N	AF	DR	Opt	LR	N.o.E	KF
DKL$_1$	600	Tanh	0.99	4	Linear	—	—	—	—	—	—	—	—	—	—	Adam	0.005	1750	RBF
DKL$_2$	160	Tanh	0.99	600	Tanh	0.99	4	Linear	—	—	—	—	—	—	—	Adam	0.005	1750	RBF
DKL$_3$	160	Tanh	0.99	160	Tanh	0.99	600	ReLU	0.99	4	Linear	—	—	—	—	Adam	0.005	1750	RBF
DKL$_4$	160	Tanh	0.99	160	Tanh	0.99	600	ReLU	0.99	600	ReLU	0.99	4	Linear	—	Adam	0.005	1750	RBF
DKL$_5$	160	Tanh	0.99	600	Tanh	0.99	600	ReLU	0.99	600	ReLU	0.99	4	Linear	—	Adam	0.005	1750	RBF

[a] Number of neurons – N.o.N, activation function – AF, dropout rate – DR, optimizer – Opt, learning rate – LR, number of epochs – N.o.E, kernel function – KF.
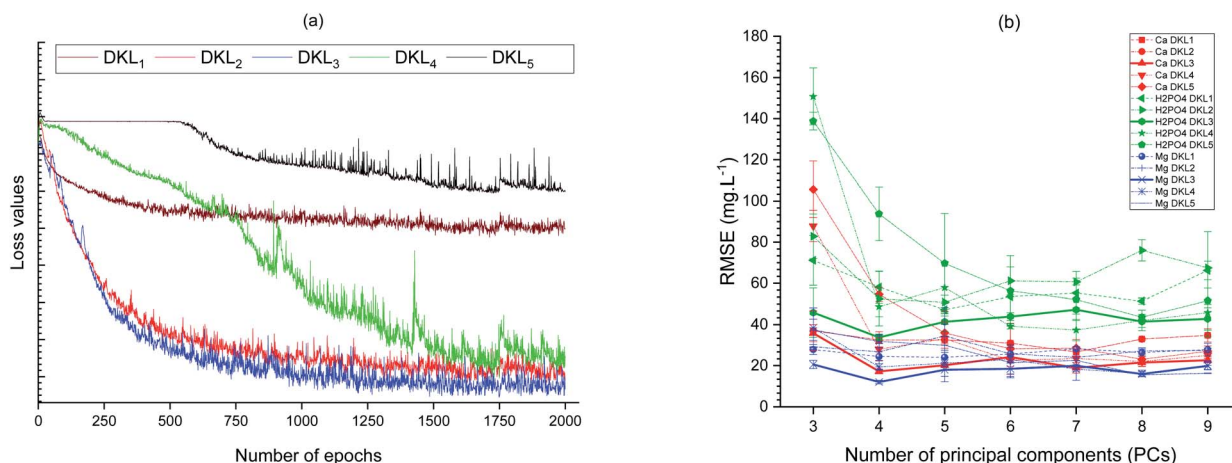

Fig. 5 Relationship between the number of epochs and loss values of the models (a), and between PC components and variance of the dataset with RMSEs (b).

ANN stage of DKL was constructed by the Tanh, ReLU, and linear activation functions. The dropout algorithm was applied to train the network to eliminate overfitting problems and local minima. Adam optimizer and standard mean squared error loss function were adopted for tuning the model.[29] Furthermore, to evaluate the most effective model for determining the three ions in the hydroponic nutrient solution, five DKL (DKL_1 to DKL_5) structures with layers, and nodes were explicitly tuned to determine the suite DKL structure for developing the SDT architecture (Table 6).

A comparison of the loss values of five cases of DKL architectures corresponding with the number of epochs change is depicted in Fig. 5a. The DKL_3 was the best fit structure for SDT because of its lowest loss value. The number of neurons of the last layer of the ANN stage was determined by trading-off the root mean square error values of predicting three ions and the coefficient of principal component (PC) analyzed from the high dimensional data of the AMSAM-FE. Removing PCs from the raw allows the models to eliminate the noise[30] and improve predicting targeted ions. The relationship between the number of PCs and the prediction RMSEs of three ions are illustrated in Fig. 5b. The RMSEs of the models achieved the minima values at 4 PCs, and the DKL_3's RMSEs values are the lowest (Fig. 5b).

3.2. Performance of DKL with lab samples

The prediction of calcium ion was more stable and linear for DKL_3 (RMSE 17.63 mg L^{-1}, R^2 0.99, and slope 1.005) than for other DKL structures (Fig. 6a). The DKL_1 showed a slightly good linear relationship (RMSE 27.02 mg L^{-1}, R^2 0.97, and slope 0.93), which was approximate to that of DKL_4 (RSME 28.02 mg L^{-1}, R^2 0.96, and slope 0.97) but relatively better than those of the DKL_2 (RSME 32.52 mg L^{-1}, R^2 0.96, and slope 0.97) and DKL_5 (RSME 54.91 mg L^{-1}, R^2 0.92, and slope 0.86) models.

Akin to calcium, the phosphate prediction of DKL_3 was good too. The DKL_3 exhibited enhanced results with lower RMSEs (33.71 mg L^{-1}), higher performance coefficient (0.99), and better slope (0.98). The performance of DKL_4 for predicting phosphate was better than those of DKL_1, DKL_2, and DKL_5. The phosphate prediction of DKL_5 was the worst with the highest RMSEs and the low linear relationship (RSME 93.79 mg L^{-1}, R^2 0.92, and slope 0.82).

The DKL_3 exhibited good prediction results not only for available ISE ions (Ca^{2+}, $H_2PO_4^-$) but also for unavailable ISE ion (Mg^{2+}). The magnesium prediction of DKL_3 was satisfactory with relatively low RMSEs, good performance coefficient, and slightly higher slope (RSME 12.51 mg L^{-1}, R^2 0.92, and slope 0.86). The magnesium prediction result of DKL_4 was better than those of DKL_1, DKL_2, and DKL_5. However, the performance of DKL_4 (RSME 17.36 mg L^{-1}, R^2 0.91, and slope 0.88) was still lower than that of DKL_3. The relationships of the predicted concentrations (y) and the actual values (x) of the models are summarized in Table 6.

3.3. In-line application of the smart diagnostic tool in lettuce hydroponic system

3.3.1. Implementing deep kernel learning in LabVIEW. A trained deep kernel learning is a computational model. It consists of a deep neural network with interconnected neurons.

Every neuron in a layer is connected to the neurons of the previous layer. The connections between layers have different strengths or weights. The input data enter and pass-through layer by layer up to the output. In this study, the DKL was implemented in LabVIEW, which is an advanced language and can be applied in a real-time system.[31] The weights and biases of
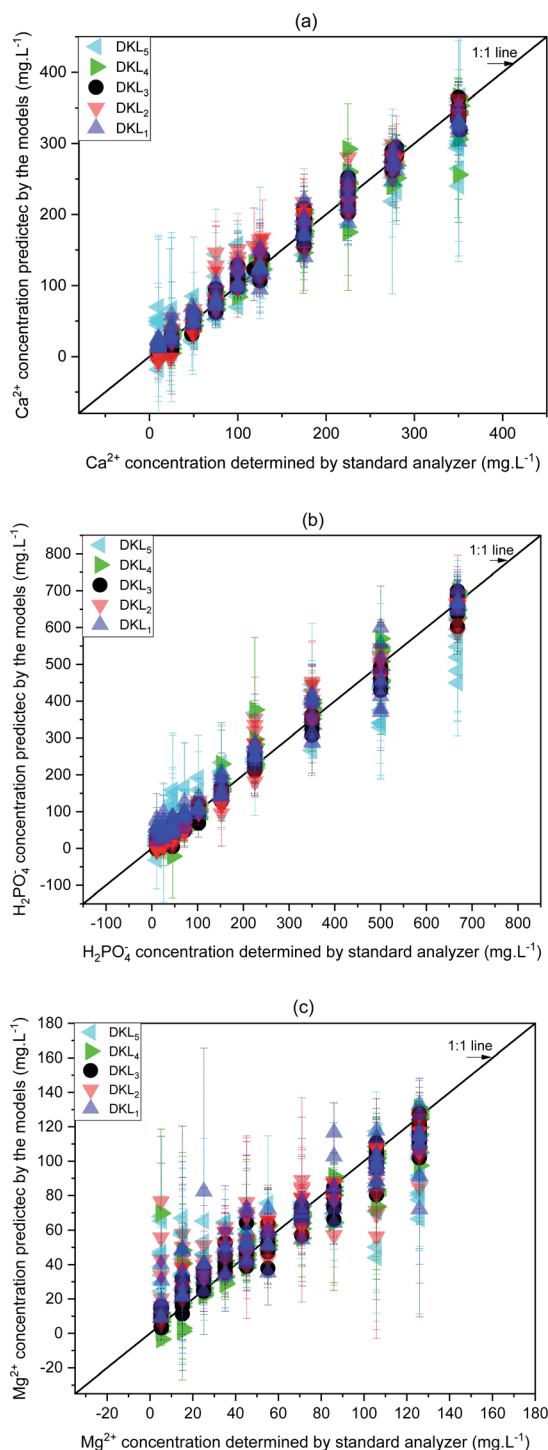

Fig. 6 Relationships between predicted ion concentrations of the DKL model and standard analyzers. (a) Ca^{2+}, (b) $H_2PO_4^-$, and (c) Mg^{2+}. Error bars are three replicates' standard deviations.

Table 6 The relationship of the predicted concentrations (y) and the actual values (x) of the models

Species	Models	Predicting equation	RMSE[a] (mg L^{-1})	Coefficient of performance[b] (R^2)
Calcium	DKL$_1$	$y = 0.93x + 11.81$	27.02	0.97
	DKL$_2$	$y = 0.97x + 9.92$	32.52	0.96
	DKL$_3$	$y = 1.005x - 0.21$	17.63	0.99
	DKL$_4$	$y = 0.97x + 4.08$	28.02	0.96
	DKL$_5$	$y = 0.86x + 19.58$	54.91	0.92
Phosphate	DKL$_1$	$y = 0.93x + 27.17$	58.22	0.97
	DKL$_2$	$y = 1.006x + 2.24$	52.48	0.97
	DKL$_3$	$y = 0.98x - 1.28$	33.71	0.99
	DKL$_4$	$y = 1.02x + 3.58$	48.67	0.98
	DKL$_5$	$y = 0.82x + 35.99$	93.79	0.92
Magnesium	DKL$_1$	$y = 0.74x + 17.07$	22.43	0.85
	DKL$_2$	$y = 0.66x + 22.76$	24.25	0.80
	DKL$_3$	$y = 0.86x + 7.65$	12.51	0.92
	DKL$_4$	$y = 0.88x + 5.17$	17.36	0.91
	DKL$_5$	$y = 0.51x + 30.24$	29.79	0.65

[a] The RMSE $= \sqrt{\dfrac{1}{n}\sum_{i=1}^{n}(y_i - \hat{y}_i)^2}$, where n is the total number of data in the training set or test set, y_i is the actual ion concentration value, and $\hat{y}_i$ is the predicted ion concentration value. [b] the $R^2 = 1 - \dfrac{\sum_i (y_i - \hat{y}_i)^2}{\sum_i (\bar{y}_i - \hat{y}_i)^2}$, where $\bar{y}_i$ is the average of the test set.

the deep neural network stage and the α parameters of the GP stage were fixed after the generation of the trained model. They were saved in the form of .text files in the computer hard drive. A trained DKL model consists of input processing, layer 1, layer 2, layer 3, layer 4, GP layer, and output processing stage.

The implementation of these blocks in LabVIEW are explained with the help of mathematical equations as follows.

(a) Normalization input process. As mentioned above, the dataset fed DKL was scaled in the range of [−1 to 1] based on MinMaxScaler of the Scikit Learn library. In the LabVIEW platform, the scaled data (d_{scaled}) was also calculated from the maximum value of data (d_{max}), the minimum value of data (d_{min}), the range between d_{max} and d_{min} ($d_{\text{range}} = d_{\text{max}} - d_{\text{min}}$), the minimum of scaled value (scale$_{\text{min}}$ = −1), and the maximum of scaled value (scale$_{\text{max}}$ = 1). The d_{scaled} is computed as follows

$$d_{\text{scaled}} = \frac{(d - d_{\text{min}})}{d_{\text{range}}}(\text{scale}_{\text{max}} - \text{scale}_{\text{min}}) + \text{scale}_{\text{min}} \quad (9)$$

Eqn (9) is implemented in LabVIEW for the scaling of input vectors. The implementation is done using mathematical pallets such as divider, subtracter, adder, minima, and maxima.

(b) Layer 1. The output ($d_{\text{scaled}} = X_1$) of the normalization input processing stage was given to the inputs of layer 1. The weight and bias matrices of layer 1 of the trained DKL were saved as .txt files for implementing the model in LabVIEW. The first layer of DKL performed by sub-program in LabVIEW follows eqn (10)

$$O_{\text{layer1}} = \text{Tanh}(W_1 X_1 + b_1) \quad (10)$$

Some math tools from the numeric pallet in LabVIEW were used. The weights (W_1) were multiplied with the inputs data X_1. The production result was added with the biases. The result of this addition was then transformed with a Tanh activation function $\left(f(z) = \dfrac{2}{1 + e^{-2z}} - 1\right)$.

(c) Layer 2. Weight (W_2) and bias (b_2) matrices of layer 2 saved in .text files were imported in LabVIEW for calculating the second layer of DKL. The output of layer 1 ($O_{\text{layer1}} = X_2$) was given to layer 2. Thus the output of layer 2 is given by eqn (11)

$$O_{\text{layer2}} = \text{Tanh}(W_2 X_2 + b_2) \quad (11)$$

The sub-program was also implemented in LabVIEW using the numeric pallet, such as a multiplier, adder, and Tanh function.

(d) Layer 3. Weight (W_3) and bias (b_3) matrices of layer 3 saved in .text files were further imported in LabVIEW for calculating the third layer of DKL. The output of layer 2 (O_{layer2}) was given to layer 3 input (X_3). Hence the output of layer 3 is presented by eqn (12)

$$O_{\text{layer3}} = \text{ReLU}(W_3 X_3 + b_3) \quad (12)$$

The sub-program was also implemented in LabVIEW using the numeric pallet, such as multiplier, adder, and ReLU function $\left(f(z) = \left\{ \begin{array}{ll} 0, & z < 0 \\ z, & z \geq 0 \end{array} \right\}\right)$.

(e) Layer 4. Similarly, weight (W_3) and bias (b_3) matrices of layer 4 saved in .text files were imported in LabVIEW for calculating the fourth layer of DKL. The output of layer 3 (O_{layer3}) was given to layer 4 (X_4). So the output of layer 4 is shown by eqn (13). The sub-program was also implemented in LabVIEW using the numeric pallet, such as multiplier, adder, and linear function.
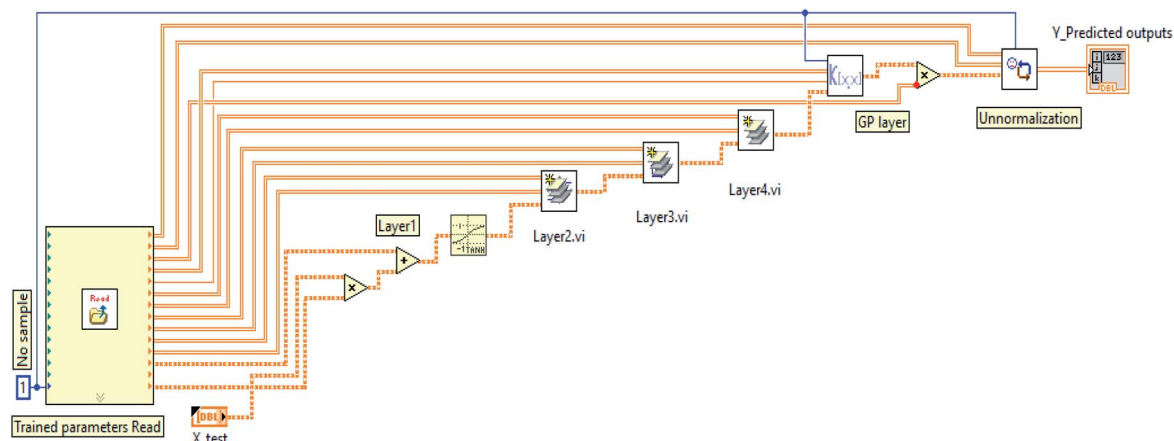
Fig. 7 The block diagram of the DKL core of the smart diagnostic tool implemented in LabVIEW.

$$O_{layer4} = linear(W_4 X_4 + b_4) \tag{13}$$

(f) GP stage. The predicted outputs are computed following eqn (15). That is the product of the covariance matrix of testing data (X_*) and training data (X) and the trained hyperparameter ($\alpha_{trained}$)

$$y_{predicted} = K(X_*,X)[K(X,X) + \delta_n{}^2 I]^{-1} y \tag{14}$$

$$y_{predicted} = K(X_*,X)\alpha_{trained} \tag{15}$$

The sub-program was also implemented in LabVIEW by using the numeric pallet, such as product matrix function.

(g) Un-normalization output process. This stage was used to un-normalize the signal from GP output. The values of targets ($d_{unscaled}$) were calculated by simple functions (*i.e.*, division,

subtraction, multiplication, and addition), as the following eqn (16).

$$d_{unscaled} = \frac{(d_{scaled} - scale_{min})}{(scale_{max} - scale_{min})} d_{range} + d_{min} \tag{16}$$

The block diagram of the DKL of the SDT is depicted in Fig. 7. Where X_test = d_scaled comes from the normalization subprogram, Y_predicted output is the target.

Fig. 8 reveals the front panel of the SDT. The sample setting area, including the numeric controls and the button controls could be used to set the standard concentrations of the three considered ions, and pump the solutions (KHP, sample, and rinse solutions) in automated/manual (Au/Man) mode. The predicted concentrations of the three target ions were displayed on the numeric indicators (current ion concentrations area) and
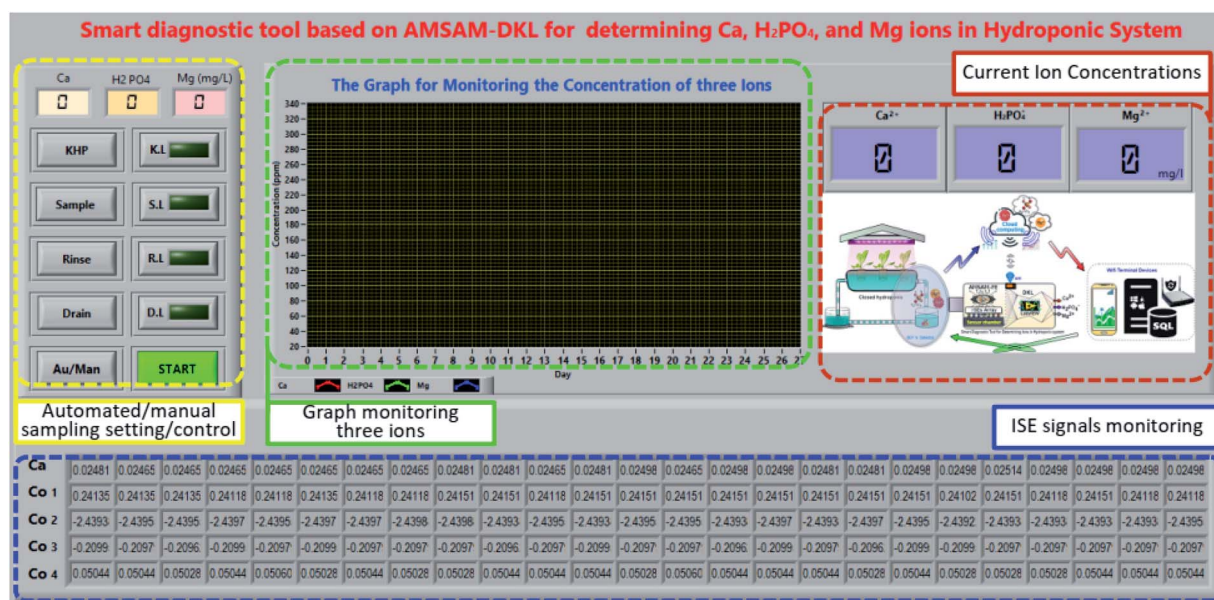

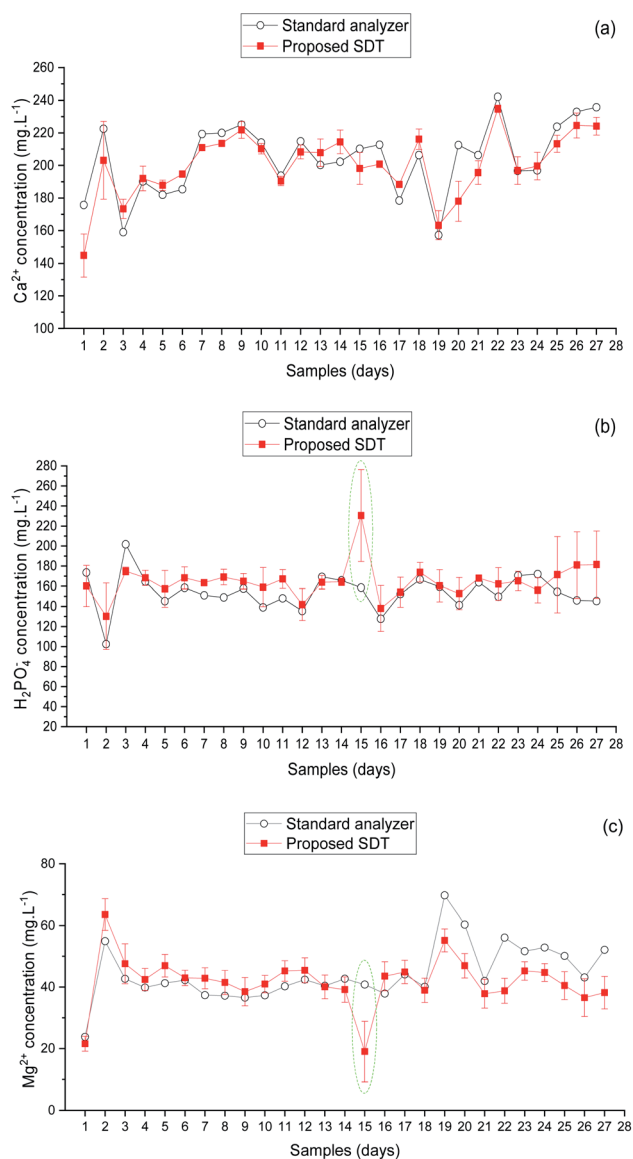**Fig. 8** The front panel of the smart diagnostic tool implemented in LabVIEW.

Fig. 9 Comparison between predicted ion concentrations of the smart diagnostic tool and standard analyzers. (a) Ca^{2+}, (b) $H_2PO_4^-$, and (c) Mg^{2+}. Error bars are three replicates' standard deviations.

the graph (graph monitoring the three ions area). Besides, the ISEs' EMF was indicated on the ISE signals monitoring area.

3.3.2. On-site validating the AMSAM-DKL-based SDT. After implementing the AMSAM-DKL structure in the LabVIEW platform, the SDT was validated by deploying an on-site measurement of the ions (calcium 150 to 250 mg L^{-1}, phosphate 100 to 200 mg L^{-1}, and magnesium 20 to 70 mg L^{-1}) in the nutrient solution of lettuce crop planted in the experimental plant factory of the College of Information and Electrical Engineering, China Agricultural University (CIEE, CAU), Beijing, China. The AMSAM task of SDT automatically acquired each sample per day. The predicted results of the three ions of the 27 samples are depicted in Fig. 9 and Table 7.

The calcium prediction results are illustrated in Fig. 9a and Table 7. The results of four DKL showed a relatively accurate

prediction with RMSE of 29.2, 17.9, 19.3, and 25.1 mg L^{-1} and CV of 8.9, 8.8, 9.2, and 11.2%, for DKL$_1$, DKL$_2$, DKL$_4$, and DKL$_5$, respectively. The result of DKL$_3$ was the best with the lowest RMSE of 12.4 mg L^{-1} and a CV of 4.1%.

Fig. 9b and Table 7 present the prediction results of phosphate ion of the proposed models. The graphs have a trend similar to that of calcium. However, the accuracy of phosphate prediction was slightly lower than that of calcium. The RMSEs were 25.7, 18.2, 12.1, 24.1, and 27.8 mg L^{-1} with CVs of 12.1, 9.8, 6.2, 10.8, and 26.6%, for DKL$_1$, DKL$_2$, DKL$_3$, DKL$_4$, and DKL$_5$, respectively. Specifically, the error prediction of phosphate at the 15$^{\text{th}}$ sample raised sharply. Nevertheless, the precision of phosphate prediction was satisfactory for determining H$_2$PO$_4^-$ element in the hydroponic system.

The magnesium prediction results are shown in Fig. 9c and Table 7. The results of four DKL models (RMSEs of 17.2, 10.5, 11.0, and 13.8 mg L^{-1} with respective CVs of 18.1, 11.9, 16.3, and 56.6%, for DKL$_1$, DKL$_2$, DKL$_4$, and DKL$_5$, respectively) showed lower accuracies than those of the DKL$_3$ (RMSE of 7.5 mg L^{-1} with CV of 9.6%). At the 15$^{\text{th}}$ sample, the prediction error of magnesium was substantially higher than those of other samples. The fluctuated magnesium prediction trend was similar to phosphate. However, the trends were opposite (Fig. 9b and c).

4. Discussion

We modeled and implemented a smart diagnostic tool for on-site concentrations measurement of the three ions in a hydroponic system. The core of the SDT was a combination of the AMSAM-FE sampling method and the DKL model. The novel on-site measurement with this approach could overcome the drawbacks of ISEs for determining the concentration of available ISEs ion (Ca) and unavailable ISEs ions (P and Mg). The results showed that the SDT could be used to online-measure three ions in the hydroponic system with a relatively satisfactory accuracy. However, at the 15$^{\text{th}}$ sample, the achieved phosphate and magnesium predictions were not high accuracies (see Fig. 9b and c). These errors may be due to an issue with the reference electrode (RE). The inner solution of RE ran out in order to reach the lowest level. That affected the EMF of Co-electrodes over the trained range and caused the inaccuracy predictions. The variating EMF of Co-ISEs also induced inaccuracy in magnesium prediction since magnesium concentration was predicted by fusing the signals from Co-electrodes and calcium electrode (CE). However, the calcium prediction was still stable because CE is a combination electrode (*i.e.*, it has its own independent RE). This is an advantage of the combination electrode technique.

The accuracy predictions of the three ions in the on-site measurement task were considerably high. Although slightly lower than those of the training stage, the results showed that the AMSAM developed by low-cost and straightforward components (such as, a Lab 3D printed sensor chamber and a low-cost peristaltic pump (pump A), *etc.*), was still efficient for developing an affordable and applicable SDT architecture. Fig. 10 illustrates the characteristics of the pump-based sample

Table 7 A comparison of the predicted quality of the proposed models with the real hydroponic solution tests

Considered Ions	Range of concentration (mg L^{-1})	Models	Accuracy (RMSE, mg L^{-1})	Precision (CV^a,%)
Calcium	150 to 250	DKL$_1$	29.2	8.9
		DKL$_2$	17.9	8.8
		DKL$_3$	12.4	4.1
		DKL$_4$	19.3	9.2
		DKL$_5$	25.1	11.2
Phosphate	100 to 200	DKL$_1$	25.7	12.1
		DKL$_2$	18.2	9.8
		DKL$_3$	12.1	6.2
		DKL$_4$	24.1	10.8
		DKL$_5$	27.8	26.6
Magnesium	20 to 70	DKL$_1$	17.2	18.1
		DKL$_2$	10.5	11.9
		DKL$_3$	7.5	9.6
		DKL$_4$	11.0	16.3
		DKL$_5$	13.8	56.6

^{a} $\text{CV} = \dfrac{\text{SD}}{\bar{y}_N} \times 100 = \dfrac{\sqrt{\dfrac{\sum_i^N (\hat{y}_i - \bar{y}_s)^2}{N-1}}}{\bar{y}_N \times 100}$ with the standard deviation (SD), the average concentration of samples ($\bar{y}_s$), the average concentration of measurements ($\bar{y}_N$), and the number of samples (N).

quantification. Significant linear relationships were found between volumes set by the pumps and the standard volume having small RMSEs of 0.45 and 0.14 mL, CV of 3.1 and 1.2%, and high R^2 of 0.9986 and 0.9996 for pump A, pump B, respectively. Furthermore, the results of calcium and phosphate prediction proved that the automated sampling technique based on AMSAM contributed significantly towards the improvement in the prediction accuracy of the two elements. Pre-processing based AMSAM-FE eliminated negative factors, for example, the interferences of ionic strength fluctuation, the matrix background of solution change,[4,14] the variation of EMFs (*i.e.* the fluctuated potentials of ISEs while moving them from the sample to the other solutions[32]). The samples were regulated

Fig. 10 The relationship between the volumes set by pumps and standard volume.

at ~5.0 pH, which facilitated calcium and phosphate ISEs to work well. The feature enrichment signals furnished extra information to the DKL model to improve the three ions prediction accuracies.

The burden of computation was an inherent disadvantage of the general DKL.[25] Due to this drawback, DKL was not deployed effectively in the real-time application. On the other hand, LabVIEW is a powerful graphic (G) language that works well with data flow architecture, visual programming, parallel processing, and special real-time interface with the semi-nature system (a system that combines both physical and virtual equipment).[31] In this study, LabVIEW was utilized to implement and alleviate the shortcoming of the proposed DKL. Tuning the hyper-parameters (number of hidden layers, number of nodes in each layer, *etc.*) is the most complicated task in developing the machine learning models. In this experiment, the relationship between the principal components (PCs) of the raw ISEs' data and the RMSEs of the performed models was evaluated to visualize the models' optimizing targets. That can be used to reduce the modeling progress's optimization burden. In general, the fewer the nodes of the last layer of the DNN, the quicker computation of DKL was. Nevertheless, the number of neurons in the last layer of the DNN also affected the DKL performances. Specifically in this scenario, the magnesium is not an available ISEs element. The predicted concentration of magnesium ion depended on both the available ISEs' signals (calcium and phosphate). Therefore, in the few PCs case, original magnesium information in the DNN's output data (the GP input data) may be reduced. That reduces the accuracy of magnesium prediction (Fig. 5 at PCs = 3). Whereas in the 9-PCs case, the model performance was not satisfactory either. The high numbers of PCs mean that the dimensions of given data to
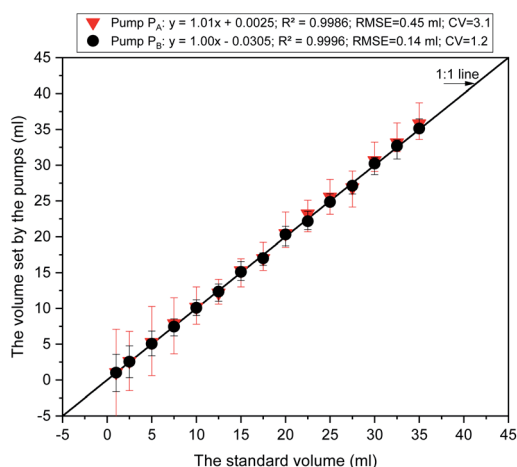
the GP stage were high, affecting the DKL models' accuracies.[4] The fitted PCs were four at which the RMSEs of the models were minima (Fig. 5b). Moreover, comparing five DKL structures supplied the basis to choose the suitable DKL architecture for the SDT. The DKL_1 and DKL_2 were constructed with a relatively small DNN core that allows deploying conveniently and fast. However, their performances were not satisfactory because they could not generalize the targets with slightly small data samples in this scenario. The DKL_4 and DKL_5 architectures achieved relatively satisfactory results. Nevertheless, their big DNN core makes implementing the DKL more complicated and unsuitable for real-time processing requirements. DKL_3 was the best model for the SDT. It was a slightly compactable architecture 160-160-600-4-GP (a 160-160-600-4 neural network and a GP stage). The DKL_3-based SDT was implemented successfully in LabVIEW platform and worked well with just about 100 milliseconds processing time based on a personal computer (Asus K401L, CPU core i5 2.7 GHz). The DKL_3 core was combined with an AMSAM sampling module to build up the SDT by which the three ions (calcium, phosphate, and magnesium) were determined on-site timely.

The fitted DKL structure was verified using the lab samples (Fig. 6) and the real on-site samples (Fig. 9). The performance of DKL_3 was better, linear and with lower errors than the other models. Specifically, the results of the training stage (Fig. 6 and Table 6) exhibited that DKL_3 was the accomplished model for the SDT, and was trained well with a high coefficient of performance R^2 (0.99) and a slope ($\sim$1.0) for calcium. Although the big error occurred at the 15th sample (see Fig. 9) by the draining out of the RE's filling solution, this error could be
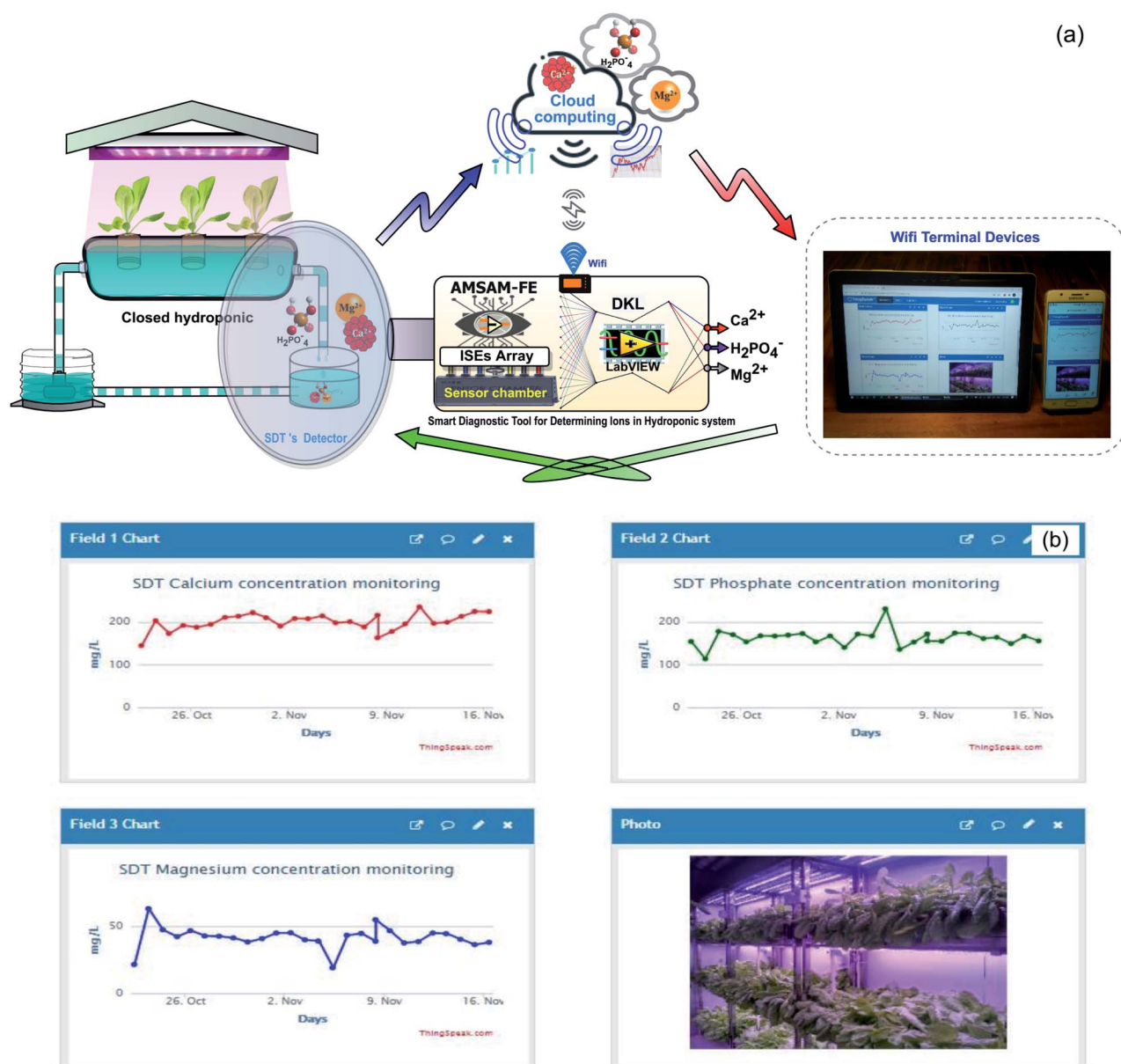

Fig. 11 Concentrations of the three ions updated on Thingspeak Web verified SDT feasibility in the field.

eliminated by maintaining the inner solution at a suitable level. Therefore, the results of SDT with the real on-site sample from the lettuce hydroponic system were evaluated with 26 samples. DKL_3 was the suitable core with the lowest RMSE of 12.4, 12.1, and 7.5 mg L^{-1} and the lowest CVs of 4.1, 6.2, and 9.6% for predicting calcium, phosphate, and magnesium, respectively (Fig. 9, and Table 7). The satisfying results of DKL_3 for determining the concentration of the three ions in the real on-site lettuce hydroponic system proved that DKL-based SDT was implemented entirely in the LabVIEW platform based on the regular functions and Virtual Instruments (VIs). DKL-LabVIEW-based SDT results demonstrate that DKL could be deployed efficiently in the third environment without the complicated machine learning toolkits.

Moreover, the opened connectivity capability of the proposed SDT allows to update data (with determined ions concentration) to cloud computing based on Thingspeak, an open internet of things (IoT) service (IoBridge, Marlborough, MA, USA). The growers can access SDT's database from any static or mobile device (computers or smartphones *etc.*) *via* the Web platform. The posted data from SDT are updated per every 15 seconds of time. It is entirely applicable for deploying the remote monitoring system, the IoT-based control system in big modern agricultural projects. SDT can also work well as an intelligent edge computing supplied diagnosed nutrient information and plant growth stage for the 4.0 technology-based agriculture systems.[21] Fig. 11 presents the application of SDT in the lettuce hydroponic system (Fig. 11a) and the predicted concentration of the three ions (Fig. 11b).

5. Conclusion

We developed a smart diagnostic tool for on-site determination of three ions concentration in lettuce hydroponic nutrient solution. The DKL model core of SDT was developed in Python and implemented in the real-time environment (LabVIEW) to undertake the real on-site diagnostic tasks. The AMSAM-FE based acquiring and preprocessing of data and the DKL model were incorporated for developing the SDT that could quantify the concentration of calcium, phosphate, and magnesium on-site. Hardware sampling technique and software signal processing were applied in combination to improve the accuracy of the measurements by resolving the disadvantages of ISEs, for example, signal drifts, interferences, and ionic strength.[4]

The AMSAM developed by the low cost and simple components, such as a 3D printed sensor chamber, two electromagnetic valves, a tiny electric pump, and two peristaltic pumps, effectively sampled and significantly contributed towards improving the accuracy of the SDT. Moreover, the DKL model supported by the MSAM-FE could be modeled satisfactorily with only 100 Lab-synthesized samples. The SDT structure's feasibility was evaluated in the actual lettuce hydroponic system with the real hydroponic solution.

The complicated computation of deploying the DKL in the field was implemented successfully in the LabVIEW for the first time. This exhibits that the DKL can be exploited in solving

problems in on-site ions (Ca, P, Mg) concentrations measurement in the actual hydroponic system. This study also showed that the three ions were effectively and accurately diagnosed in real-time by the smart diagnostic tool. The SDT could be used as a component for automated monitoring of plants nutrients in a hydroponic system. It could also be employed in smart sensing that would supply useful information of the three elements to growers or managers for manipulating the hydroponic system through the cloud computing database of on-site measurement of these ions. Moreover, this study suggests that the SDT can be deployed for improving the quality of modern agriculture based on hydroponics and internet of things (IoT) backbone.

This approach proved that the DKL could be implemented in the third environment without the complicated Toolkits or Libraries. That also paved the way for applying the DKL in a real system based on low-cost and straightforward hardware and software platforms.

The results of the proposed approach were rather good with RMSE of 12.5, 12.1, and 7.5 mg L^{-1} and the CV% of 4.1, 6.2, 9.8 for predicting calcium, phosphate, and magnesium in the range of 150–250, 100–200, and 20–70 mg L^{-1}, respectively. The accuracy of magnesium prediction was slightly lower than those of calcium and phosphate. However, in the unavailable magnesium ISE condition, this approach could still supply magnesium trace for improving the fertilizer management efficiency in a real hydroponic system.

Author contributions

The manuscript was written through contributions of all authors. All authors have given approval to the final version of the manuscript.

Funding

Conflicts of interest

The authors declare no conflict of interest.

Acknowledgements

References

1 H. Zekki, L. Gauthier and A. Gosselin, *J. Am. Soc. Hortic. Sci.*, 1996, **121**, 1082–1088.

2 M. T. Ko, T. I. Ahn, Y. Y. Cho and J. E. Son, *Hortic., Environ. Biotechnol.*, 2013, **54**, 412–421.

3 D. H. Jung, H. J. Kim, W. J. Cho, S. H. Park and S. H. Yang, *Comput. Electron. Agric.*, 2019, **156**, 660–668.

4 T. Vu Ngoc, A. M. Khattak, H. Zhu, W. Gao and M. Wang, *Sensors*, 2020, **20**, 5314.

5 H.-J. Kim, W.-K. Kim, M.-Y. Roh, C.-I. Kang, J.-M. Park and K. A. Sudduth, *Comput. Electron. Agric.*, 2013, **93**, 46–54.

6 J. Saurina, E. López-Aviles, A. Le Moal and S. Hernández-Cassou, *Anal. Chim. Acta*, 2002, **464**, 89–98.

7 L. Wang, Y. Cheng, D. Lamb, P. J. Lesniewski, Z. L. Chen, M. Megharaj and R. Naidu, *J. Chemom.*, 2017, **31**, e2870.

8 W. J. Cho, H. J. Kim, D. H. Jung, H. J. Han and Y. Y. Cho, *Sensors*, 2019, **19**, 17.

9 A. C. Wilson and K. H. Pool, *Anal. Chim. Acta*, 1979, **109**, 149–155.

10 S. A. Glazier and M. A. Arnold, *Anal. Chem.*, 1991, **63**, 754–759.

11 R. Marco and P. Alexander, *Anal. Commun.*, 1997, **34**, 93–95.

12 D.-H. Jung, H.-J. Kim, H. S. Kim, J. Choi, J. D. Kim and S. H. Park, *Sensors*, 2019, **19**, 2596.

13 W. J. La, K. A. Sudduth, H. J. Kim and S. O. Chung, *Trans. ASABE*, 2016, **59**, 787–794.

14 V. N. Tuan, T. D. Dinh, A. M. Khattak, L. Zheng, X. Chu, W. Gao and M. Wang, *IEEE Access*, 2020, **8**, 28289–28300.

15 J. Saurina, E. Lopez-Aviles, A. Le Moal and S. Hernandez-Cassou, *Anal. Chim. Acta*, 2002, **464**, 89–98.

16 M. Maj-Zurawska and A. Lewenstam, *Talanta*, 2011, **87**, 295–301.

17 W. Zhang, L. Jenny and U. E. Spichiger, *Anal. Sci.*, 2000, **16**, 11–18.

18 L. Wang, D. Yang, C. Fang, Z. L. Chen, P. J. Lesniewski, M. Mallavarapu and R. Naidu, *Talanta*, 2015, **131**, 395–403.

19 H. B. Atas, A. Kenar and M. Tastekin, *Talanta*, 2020, **217**, 121110.

20 R. De Marco, B. Pejcic and Z. L. Chen, *Analyst*, 1998, **123**, 1635–1640.

21 ThingSpeak, https://thingspeak.com/, accessed on 8th October 2020.

22 L. I. Trejo-Téllez and F. C. Gómez-Merino, in *Hydroponics-A Standard Methodology for Plant Biological Researches*, InTech, 2012.

23 A. Conagin, D. Barbin, S. S. Zocchi and C. G. B. Demétrio, *Rev. Bras. Biomet.*, 2014, **32**, 180–189.

24 J. Magalhaes and A. Machado, *Analyst*, 2002, **127**, 1069–1075.

25 A. G. Wilson, Z. T. Hu, R. Salakhutdinov and E. P. Xing, in *Artificial Intelligence and Statistics*, ed. A. Gretton and C. C. Robert, Microtome Publishing, Brookline, 2016, vol. 51, pp. 370–378.

26 C. E. Rasmussen and C. Williams, *Gaussian Processes for Machine Learning*, Cambridge, MA, 2006.

27 R. M. Neal, *Bayesian learning for neural networks*, Springer Science & Business Media, 2012.

28 N. Srivastava, G. Hinton, A. Krizhevsky, I. Sutskever and R. Salakhutdinov, *J. Mach. Learn. Res.*, 2014, **15**, 1929–1958.

29 I. Goodfellow, Y. Bengio and A. Courville, *Deep learning*, MIT Press, 2016.

30 L. Wang, Y. Cheng, D. Lamb, Z. Chen, P. J. Lesniewski, M. Megharaj and R. Naidu, *Environ. Technol. Innovation*, 2016, **6**, 165–176.

31 R. Bitter, T. Mohiuddin and M. Nawrocki, *LabVIEW: Advanced programming techniques*, CRC Press, 2017.

32 C. C. Rundle, http://www.nico2000.net/Book/Guide1.html, Consulté le 14-sept-2013, 2000.